Title: Binding of SARS-CoV-2 spike protein to ACE2 is disabled by thiol-based drugs; evidence from *in vitro* SARS-CoV-2 infection studies.

One Sentence Summary: Thiol-based drugs decrease binding of SARS-CoV-2 spike protein to its receptor and inhibit SARS-CoV-2 cell entry.

Authors: Kritika Khanna[1*], Wilfred Raymond[1*], Annabelle R. Charbit[1], Jing Jin[3], Irina Gitlin[1], Monica Tang[2], Hannah S. Sperber[3], Sergej Franz[3], Satish Pillai[3,4], Graham Simmons[3,4], and John V. Fahy[1,2*].

[*]Equal Contribution

Affiliations:
[1]Cardiovascular Research Institute, University of California San Francisco, San Francisco, California.
[2]Division of Pulmonary, Critical Care, Allergy and Sleep and the Department of Medicine, University of California San Francisco, San Francisco, California.
[3]Vitalant Research Institute, San Francisco, California.
[4]Department of Laboratory Medicine, University of California San Francisco, San Francisco, California.

Abstract: Coronavirus disease 2019 (COVID-19) is caused by the severe acute respiratory syndrome coronavirus 2 (SARS-CoV-2), and the SARS-CoV-2 spike protein is an envelope glycoprotein that binds angiotensin converting enzyme 2 as an entry receptor. The capacity of enveloped viruses to infect host cells depends on a precise thiol/disulfide balance in their surface glycoprotein complexes. To determine if cystines in the SARS-CoV-2 spike protein maintain a native binding interface that can be disrupted by drugs that cleave cystines, we tested if thiol-based drugs have efficacy in receptor binding and cell infection assays. We found that thiol-based drugs, cysteamine and WR-1065 (the active metabolite of amifostine) in particular, decrease binding of SARS-CoV-2 spike protein to its receptor, decrease the entry efficiency of SARS-CoV-2 spike pseudotyped virus, and inhibit SARS-CoV-2 live virus infection. Our findings uncover a vulnerability of SARS-CoV-2 to thiol-based drugs and provide rationale to test thiol-based drugs, especially cysteamine and amifostine, as novel treatments for COVID-19.

Introduction

SARS-CoV-2 causes COVID-19, a multidimensional disease characterized predominantly by pneumonia that can progress to respiratory failure and death [1,2]. The envelope glycoproteins of SARS-CoV-2 include a spike glycoprotein trimer (SARS-2-S) that binds a cell surface protease (angiotensin converting enzyme 2 [ACE2]) as an entry receptor [3]. The viral envelopes of so-called type I enveloped viruses, including coronaviruses, retroviruses, and filoviruses, exhibit similar structural and mechanistic strategies for viral entry[4]. Among these viruses, the capacity of their envelope glycoproteins to mediate fusion of virus to host cell membranes depends on a precise

thiol/disulfide balance in the viral surface glycoprotein complex [5–8]. Natural and specific thiol/disulfide rearrangements in this complex can trigger conformational changes that promote virus entry [9–11], but removal of disulfide bridges by chemical reduction or by replacement of cysteines by mutagenesis can also disrupt viral binding to prevent infection. For example, chemical reduction of the S1 domain of SARS-CoV decreases its binding to ACE2 and inhibits transduction of Vero E6 cells by SARS-CoV pseudovirions, and site-directed mutagenesis replacing cystine forming cysteines with alanines in the SARS-COV spike (hereafter SARS-1-S) RBD prevents binding of ACE2 [6]. In addition, molecular dynamics simulations reveal that the binding affinity of SARS-2-S RBD for ACE2 is significantly impaired when all of the disulfide bonds of both ACE2 and SARS-2-S are reduced to thiol groups [12]. Thus, there is consistent literature that manipulation of the redox status of the cysteine-rich glycoproteins in viral envelopes can influence or impair viral cell entry. Despite this, there have been no reported attempts to use thiol-based drugs to cleave disulfide bridges as a direct anti-viral treatment strategy. Instead, the rationale to use thiol-based drugs to treat viral infection has been based on the anti-oxidant and anti-inflammatory properties of these drugs [13,14].

In this study, we considered the possibility that thiol-based drugs have direct anti-viral activity against SARS-CoV-2 by modifying SARS-2-S so that it does not bind to ACE2. Thiol-based drugs are distinct from sulfur-containing drugs, including sulfides (e.g. carbocysteine) or disulfides (e.g. disulfiram) that do not have a free thiol warhead and cannot cleave disulfide bridges. Sulfides and disulfides can form stable sulfur radicals and are good radical scavengers with antioxidant properties, and some - like disulfiram - may also inhibit cysteine protease activity relevant for viral replication [15]. There are 11 currently approved drugs with at least one functional thiol group and an additional three approved drugs whose active metabolite has a free thiol group (Table 1 and Table S1). We screened 8 of the thiol-based drugs for efficacy as entry inhibitors of SARS-CoV2.

Results

Cystine bridge map of SARS-CoV-2 spike protein

Using published data [16,17], we built a cystine bridge map of SARS-2-S and compared the amino acid alignment of the receptor binding domains (RBDs) in SARS-2-S and SARS-1-S. We noted 7 cystine bridges in the SARS-2-S1 domain (Figure 1a) and 4 conserved cystines between SARS-1-S and SARS-2-S RBD (Figure 1b). The conserved Cys467-Cys474 in SARS-1-S and Cys480-Cys488 in SARS-2-S constrain the ACE2 binding domains, and previous studies with SARS-1-S RBD have shown that mutagenesis of either homologous cysteine leads to loss of ACE-2 binding [6]. To further explore if Cys480-Cys488 in SARS-2-S might be vulnerable to chemical cleavage, we used protein modeling software to render the SARS-2-S RBD based on PDB entry 6M0J (Figure 1C). This rendering shows that Cys480-Cys488 is very near the RBD surface (Figure 1c).

Effects of thiol-based drugs on SARS-CoV-2 spike protein binding to ACE2

To test if thiol-based drugs can cleave cystines in the RBD of SARS-2-S to disrupt binding to ACE2, we exposed the RBD to 8 thiol-based drugs and then quantified ACE2 binding affinity in a plate-based binding assay. Carbocysteine was included as a negative control because it is a sulfur containing drug lacking a free thiol warhead (Table 1). Amifostine is a phosphorothioate prodrug whose dephosphorylated metabolite (WR-1065) is the active drug (Table 1 and Table S1). Conversion of amifostine to WR-1065 *in vivo* requires phosphatases absent in plate-based assays,

and WR-1065 (available as a commercial reagent) was tested together with amifostine (as a second negative control). The ACE2-SARS-2-S RBD binding assay was optimized by modifying a commercially available kit. RBD was covalently coupled to plates functionalized with primary amine-reactive maleic anhydride. ACE2 binding was then evaluated after RBD exposure to thiol-based drugs for 60 minutes (Figure 2a). We found that carbocysteine and amifostine had minimal effects on RBD binding to ACE2 except at the highest doses. All of the thiol-based drugs inhibited RBD binding to ACE2 in a dose dependent manner, but their potency varied. Penicillamine and succimer had relatively weak inhibitory effects (Supplementary Figure S1), but 2-mercaptoethane sulfonate, sodium salt (Mesna), bucillamine, cysteamine, and WR-1065 had much stronger effects (Figure 2b,c), These data provide strong support for our hypothesis that thiol-based drugs cleave cystine bridges in the SARS-2-S RBD to disrupt the native binding interface required for interaction with ACE2. To explore the stability of this disruption, we measured binding of SARS-2-S RBD to ACE2 at one and two hours post exposure to Mesna, bucillamine, cysteamine, and WR-1065. We found that the robust binding inhibition effect of these four drugs was retained for two hours after drug removal (Figure 2d), indicating that SARS-2-S cystines do not quickly re-form after thiol-drug exposure.

Effects of thiol-based drugs on entry efficiency of SARS-CoV-2 spike pseudotyped virus

To test if thiol-based drugs can inhibit the entry mediated by SARS-2-S, we tested drugs in a SARS-2-S pseudovirus entry assay. The pseudovirus particles carry SARS-2-S on the surface and enclose a viral genome of recombinant vesicular stomatitis virus (VSV) with a deleted glycoprotein (rVSV-ΔG) and an insertion of the firefly luciferase gene. In these experiments, we first exposed pseudovirus particles to thiol-based drugs and then quantified cell entry efficiency in human embryonic kidney cells (HEK293T) stably transfected to express huACE2 and transmembrane protease, serine 2 (TMPRSS2, a priming serine protease for SARS-CoV-2 [3]) (293T-ACE2-TMRPRSS2 cells). As illustrated in Figure S2, the experimental protocol measured SARS-2-S pseudovirus entry into 293T-ACE2-TMPRSS2 cells in a condition where the virus was first pre-treated with thiol-based drugs for 2 hours and a condition in which the 293T-ACE2-TMPRSS2 cells was first pre-treated with thiol-based drugs for 2 hours before transduction with the SARS-2-S pseudovirus. None of the drugs significantly affected cell viability, and pretreatment of SARS-2-S pseudovirus with carbocysteine and amifostine did not inhibit viral cell entry (Figure 3a, b), but pretreatment of SARS-2-S pseudovirus with all of the thiol-based drugs significantly decreased viral entry in a dose dependent manner (Figure 3c-h). WR-1065 and cysteamine were particularly potent entry inhibitors with efficacy apparent in low millimolar doses (Figure 3g, h). These data demonstrate that thiol-based drugs disable SARS-2-S and prevent it from interacting with ACE2. In experiments where the 293T-ACE2-TMPRSS2 cells were pretreated with thiol-based drugs and infected with untreated SARS-2-S pseudovirus, only small and inconsistent effects on pseudovirus cell entry were evident (Supplementary Figure S3).

Effects of thiol-based drugs on SARS-CoV-2 live virus infection.

To determine if thiol-based drugs inhibit entry of live SARS-CoV2 virus to host cells, we tested the four most potent drugs in the plate-binding and pseudovirus assays in a live virus assay. Specifically, SARS-CoV-2 virus was pre-treated for 2 hours with cysteamine, WR-1065, Mesna and bucillamine before infection in Vero E6 cells. Carbocysteine was again used as a negative control. We found that cytopathic effects (CPE) in virus-infected cells were inhibited by cysteamine, WR-1065, Mesna and bucillamine but not by carbocysteine (Figure 4). The inhibitory

effects of WR-1065 and cysteamine were evident at micromolar concentrations of drug whereas the inhibitory effects of Mesna and bucillamine required millimolar drug doses. Application of thiol-based drugs to cells before infection with untreated SARS-CoV2 did not inhibit CPE (Supplementary Figure S4).

Discussion

A major challenge of the COVID-19 pandemic has been to identify treatments that can address the morbidity, mortality, and economic harm caused by this disease. Our review of the amino acid sequence and crystal structure of SARS-2-S suggested that disulfides in the RBD maintain a native binding interface for interaction with ACE2 and that disrupting this interface with thiol-based drugs would be a rational and feasible antiviral strategy that could be delivered quickly. We provide support for our hypothesis with data generated in a receptor binding assay, a cell entry assay that utilizes SARS-CoV-2 spike pseudotyped virus, and a live virus cell infection assay. These different experimental approaches show that thiol-based drugs decrease binding of SARS-CoV-2 spike protein to its receptor, decrease entry efficiency of pseudotyped virus, and inhibit live virus infection. These findings uncover a vulnerability of SARS-CoV-2 to thiol-based drugs and provide rationale to test currently available thiol-based drugs as novel treatments for COVID-19.

Our data demonstrate that cystines in the RBD of SARS-2-S maintain a native binding interface that can be disrupted by thiol-based drugs to inhibit binding of SARS-2-S to ACE2 and decrease virus entry. We suspect that thiol-based cleavage of Cys480-Cys488 explains the efficacy of the thiol-based drugs as entry inhibitors of SARS-CoV2, because it is accessible at the RBD surface, but we do not provide direct evidence for the critical importance of this cystine. Cleavage of the other three cystines in the RBD could also allosterically modify the binding interface in ways that decrease binding to ACE2. Also, other cysteine residues – Cys822 and Cys833 – flanking the S2 domain mediate membrane fusion of SARS CoV1 [18] raising the possibility that thiol-based drugs could inhibit membrane fusion. In this regard, it is notable that we observed a consistent rank order for the efficacy of the different thiol-based drugs as virus entry inhibitors, and that WR-1065 and Cysteamine were the two most potent inhibitors. The rank ordering generally followed the thiol pKa values, with drugs with higher pKa (e.g. N-acetylcysteine) being least effective and drugs with lower pKa (WR-1065 and cysteamine) being most effective. The pKa value determines the fraction of active thiolate anion that participates in thiol-disulfide exchange at a given pH [19,20]. The potency of WR-1065 and cysteamine - both aminothiols - was especially notable in the cell-based virus assays and not as prominent in the plate-based binding assay. The larger effect of WR-1065 and cysteamine as compared to other thiol drugs tested in the cell-based assays may be because these two drugs more effectively cleave cystines in both S1 and S2 domains of the S protein to inhibit both receptor binding and membrane fusion. It is also possible that mechanisms other than cystine cleavage that are dependent on the presence of the positively charged amino groups are contributing to the enhanced potency of these drugs in cell-based assays.

To our knowledge, this efficacy of thiol-based drugs as direct antiviral agents has not previously been reported. Thiol-based drugs therefore represent a rational drug class to repurpose for testing in COVID-19 clinical trials. The fact that these drugs prevent viral entry is particularly appealing, because entry inhibitors prevent cell infection and interrupt active infection. Thiol-based drugs have been used for decades for multiple disease indications and are well tolerated, even at high

doses (Table S1). It is particularly appealing to re-purpose cysteamine and amifostine as COVID-19 treatments, because we show that micromolar concentrations of these dugs inhibit cell entry of SARS-CoV2. Cysteamine is used to treat cystinosis, a lysosomal storage disease characterized by cystine accumulation, and it is available in tablet (including extended release) and eye drop formulations [21,22]. Amifostine is used to treat complications of DNA-binding chemotherapeutic agents, and the trihydrate form is available as a lyophilized powder that is reconstituted for intravenous infusion [23]. Our data provide strong rationale for clinical trials to test the efficacy of cysteamine and amifostine for COVID-19. Possibilities include the oral administration of cysteamine for less severe cases of COVID-19 or for post exposure prophylaxis and intravenous administration of amifostine for treatment of more severe cases of COVID-19.

Materials and Methods

Cells, plasmids and virus

HEK293T/clone17 (CRL-11268) and Vero E6 (CRL-1586) cells were cultured in Dulbecco's Modified Eagle´s Medium (DMEM) supplemented with 10% fetal bovine serum and 1% penicillin/streptomycin (Thermo Fischer Scientific). The cells were obtained from ATCC and incubated at 37ºC and 5% CO_2. MEXi 293E cells (IBA Lifesciences) were cultured in MEXi culture medium (IBA Lifesciences) at 37ºC, 5% CO_2 and 125 RPM as described by the manufacturer. The codon-optimized SARS-CoV-2 spike gene was subcloned from pCG SARS-CoV-2 Spike (provided courtesy of Stefan Pölhmann [3]) into the EBNA-1 dependent expression vector pTT5 for high-level expression in MEXi 293E cells. To boost cell surface expression of SARS-CoV-2 spike for efficient pseudotyping VSV, the C-terminal 21 amino acid containing the ER-retrieval signal (KxHxx) of spike was deleted. Plasmids for engineering lentiviral ACE2 and TMPRSS2 expression constructs: pLKO5d.SFFV.dCas9-KRAB.P2A.BSD (a gift from Dirk Heckl, Addgene plasmid) and pDUAL CLDN (GFP) (a gift from Joe Grove, Addgene plasmid). SARS-CoV-2, isolate USA-WA1/2020 (NR-52281) was obtained from BEI resources and passaged in Vero E6 cells. Confluent Vero E6 cells grown in T175 flasks were infected with SARS-CoV-2 and the culture supernatant was collected when widespread cytopathic effect (CPE) was observed. After filtration through 0.45 µm filters, the virus containing culture supernatant was stored at -80°C in small aliquots.

Thiol-based drugs and thiol content determination

N-acetylcysteine (NAC) and MESNA were the pharmaceutical formulations, with NAC manufactured by American Reagent INC at 200mg/ml and MESNA by Baxter at 100mg/ml USP. Cysteamine (MilliporeSigma), amifostine (MilliporeSigma), WR-1065 (MilliporeSigma) and penicillamine (MP Biomedicals) were lyophilized powders that were solubilized as 500mM concentrated stocks in water. Cysteamine and WR-2065 were at pH 5. Amifostine was at pH 7 which was adjusted to pH 5. To ensure that amifostine does not auto-dephosphorylate to WR-1065, it was made fresh before the experiment each time. Bucillamine (MilliporeSigma) and tiopronin (Spectrum Chemicals) were lyophilized powders that were solubilized as 500mM concentrated stocks in equimolar NaOH to increase the solubility, and the pH was adjusted to pH 5. Carbocysteine (MilliporeSigma) and succimer (MilliporeSigma) were solubilized as 250mM concentrated stocks in 500mM NaOH to increase solubility with pH adjusted to pH 5. Free thiol

content, and thus concentration of an active drug, was measured before every experiment using Ellman's Reagent, 5,5'-dithio-*bis*-(2-nitrobenzoic acid) (DTNB) (Abcam), with the molar extinction coefficient of 14,150$M^{-1}cm^{-1}$ at 412nm[24]. Active drug concentration measured by DTNB was within 85 to 99% of nominal drug concentration. The stocks were stored at –20ºC and discarded if the thiol content went below 85%. Drug concentrations reported in plate-binding and viral entry assays are based on active drug concentration in stock.

Structure Rendering and Analysis

Space filling images and receptor distance calculations were performed using indicated PDB entries with UCSF Chimera, developed by the Resource for Biocomputing, Visualization, and Informatics at the University of California, San Francisco, with support from NIH P41-GM103311 [25].

RBD to ACE2 plate based binding assay

Amine-reactive maleic anhydride-derivatized 96-well plates were obtained from Thermo Scientific. Recombinant SARS-CoV-2 Receptor binding domain (aa 319-537, (RBD), biotinylated soluble recombinant angiotensin converting enzyme 2 (ACE2), and Streptavidin-HRP were purchased from ACRO Biosystems. TMB and stop Solution were purchased from Sera Care. Wells of maleic anhydride plates were washed three times with 200 µl wash buffer (PBS + 0.05% Tween-20, pH7.4), as will all following washes. One hundred microliters of 1 µg/ml RBD in coating buffer (0.05M carbonate-bicarbonate buffer; pH 9.6) was added to each well and incubated overnight at 4ºC, then washed. Plates were blocked with 2% BSA in wash buffer-for 60 minutes at 37ºC, then washed. Wells were incubated with 100µl of drugs at concentrations ranging from 0 to 20mM diluted in PBS, for 60 minutes at 37ºC. Negative controls included wells with no RBD or no ACE2. After washing, 100µl ACE2-biotin were added at 0.06 µg/ml in dilution buffer (PBS + 0.5% BSA + 0.05% Tween-20) and incubated at 37ºC for 60 minutes. After washing, 100µl streptavidin-HRP at 0.1µg/ml in dilution buffer were added to wells for 60 minutes at 37ºC. The plates were washed three times and incubated at 37ºC for 10 minutes in 100µl of TMB. The reaction was stopped with 0.5M hydrochloric acid stop solution and absorbance was read at 450 nm on a spectrophotometer plate reader. Absorbance readings, after subtracting from negative control wells, were transformed to percent binding, with the wells containing no drug set as 100 percent binding.

To measure the stability of binding of cysteamine, WR-1065, Mesna and bucillamine, wells were incubated with either drugs at 5mM for 1 hour, followed by three washes. ACE2 was then added to the wells either immediately, after 60 minutes, or after 120 minutes. Wells waiting for ACE2 were filled with 200µl of dilution buffer. This was followed by the same steps to assess ACE2 binding as described above. For all binding assays, 4-6 independent experiments were carried out for all drugs, with 2 replicates in each.

Production of pseudoviruses

Pseudoviruses bearing SARS-2-S were generated using recombinant VSVΔG-luciferase-based viruses, which lack glycoprotein (G) gene and instead code for reporter gene firefly luciferase. Briefly, MEXi cells were transfected with SARS-CoV-2 Spike expression plasmid (pTT5 SARS-CoV-2 SΔ21), using PEI as described by the manufacturer. Mock transfection served as the 'no glycoprotein' control. At 2-3 days post-transfection, the cells were inoculated with

VSVG/VSVΔG-luc at a multiplicity of infection (MOI) of 0.3. After 6 hours of incubation, the cells were washed twice with PBS by centrifugation and resuspended in culture medium containing 1% I1 anti-VSV-G hybridoma supernatant (ATCC CRL-2700). At 24hours post-infection, the culture supernatant was collected by centrifugation and filtered through a 0.45-µm syringe filter to clear off cellular debris. The supernatant containing viral particles was aliquoted and stored at -80 °C until further use.

Establishment of HEK293T cells stably expressing ACE2 and TMPRSS2 (293T-ACE2-TMPRSS2)

Engineering of lentiviral ACE2 and TMPRSS2 expression constructs

ACE2 and TMPRSS2 were cloned into separate lentiviral expression constructs. ACE2 was cloned into pLKO5d.SFFV.dCas9-KRAB.P2A.BSD (a gift from Dirk Heckl, Addgene plasmid) by replacing dCAS9-KRAB with new unique enzyme restriction sites (SpeI and NheI) and subsequently inserting the ACE2 gene sequence into the expression construct downstream of the SFFV promoter based on restriction enzyme cloning. TMPRSS2 was cloned into pDUAL CLDN (GFP) (a gift from Joe Grove, Addgene plasmid). GFP was exchanged with a puromycin cassette using enzyme restriction sites MluI and XhoI to enable antibiotic selection in cell culture. TMPRSS2 was inserted into the expression construct immediately downstream of the SFFV promoter following the addition of unique enzyme restriction sites (SrfI and SalI). All cloning steps were confirmed by Sanger sequencing.

Production of lentiviral particles

Lentiviral particles for delivery of lentiviral ACE2 and TMPRSS2 vectors were produced using a polyethylenimine (PEI; Polysciences, Inc) transfection protocol. Briefly, HEK293T cells were transfected with three plasmids: lentiviral ACE2 or TMPRSS2 constructs, psPAX2, and VSVg, at a ratio of 4:3:1 and a final DNA amount of 1.5 µg prepared in Opti-MEM (ThermoFisher). PEI was added at a ratio of 3:1 PEI:DNA (4.5 µg PEI). The transfection mix was vortexed and incubated for 15 min at RT and added to the cells. 16h post transfection, transfection medium was replaced with standard culture medium, and cells were cultured for another 24h. Cell supernatants containing the newly produced viral particles were then collected 48h post transfection. Supernatants were centrifuged at 4°C and subsequently filtered using 0.22 µm vacuum filter units (MilliporeSigma). The supernatants were then aliquoted and stored at -80°C.

Establishment of cells stably expressing ACE2 and TMPRSS2 (293T-ACE2-TMPRSS2)

To establish HEK293T cells stably expressing ACE2 and TMPRSS2 (293T-ACE2-TMPRSS2 cells), 0.4 x10^6 cells were seeded in 12-well plates. The following day, cells were transduced with lentiviral particles containing the ACE2 vector by adding 500 µl of lentiviral particles and 500 µl culture medium per well. 48h post transduction, medium was replaced with blastidicin (BSD; InvivoGen) selection medium at a final concentration of 10 mg/ml BSD. After 5 days of selection, cells were transferred to 75 cm^2 cell culture flasks for further expansion of cells stably expressing ACE2. The process was then repeated to further transduce cells with TMPRSS2 lentiviral particles and cells were cultured in antibiotic selection medium containing 10 µg/ml BSD and 1 µg/ml Puromycin 48h post transduction. The expression of ACE2 and TMPRSS2 was confirmed by Western Blot and compared to nontransduced cells.

Pseudovirus transduction experiments

293T-ACE2-TMPRSS2 cells were plated in black 96-well tissue culture treated plates (Greiner Bio-one) 18 hours before the experiment. Two experimental strategies of pseudovirus pre-treatment and cell pre-treatment were followed (Figure S2). For pseudovirus pre-treatment, the pseudoviruses were pre-incubated with different concentrations (1.56 -100mM) of the thiol-based drugs for 2 hours at 37ºC, followed by 66-fold dilution with standard culture media. The cells were then transduced with these pre-treated virions for 2 hours at 37ºC. After the incubation, the virions were removed and cells were cultured in standard culture medium. For cell re-treatment, the 293T-ACE2-TMPRSS2 cells were incubated with the different drug concentration (0.02 -1.5mM) for 2 hours at 37ºC, 5%CO_2. These concentrations reflect the 66-fold dilution of drugs when virus/drug mix was incubated with the cells in the pseudovirus pre-treatment experiment. After incubation, the media was removed and the cells were transduced with untreated pseudoviruses for 2 hours at 37ºC. After the incubation, the virions were removed and the cells were cultured in standard culture medium.
For both experimental conditions, at 18 hours post-transduction, the cells were lysed and luciferase activity was measured using Promega luciferase assay system and Biotek Synergy H1 plate reader. Data was normalized to the viral particles without any viral envelope protein. For each experiment, luciferase reads of no drug control group was set as 100% and the relative transduction efficiencies in the presence of thiol-based drugs were calculated. Three-four independent experiments were carried out for each PV pretreatment and cell pretreatment strategies, with 12 replicates in each for all the drug doses.

SARS-CoV-2 quantification

Titers of SARS-CoV-2 was measured by $TCID_{50}$ using Vero E6 cells. Viruses were 10-fold serially diluted in DMEM with 1% FBS prior to addition to cell monolayer in 96-well-plate. For each dilution, viruses were added to 10 replicate wells at 100 µl per well. After two hours of infection, cells were washed and cultured with fresh DMEM medium containing 1% FBS at 37˚C with 5% CO_2. Clear CPE was observed two days later. 50% endpoints were calculated with Reed and Muench method [26].

Inhibition of SARS-CoV-2 infection

SARS-CoV-2 of 1.2 x 10^4 $TCID_{50}$/ml was incubated with 2-fold serially diluted thiol-based drugs at 37°C for 2 hrs. Virus-drug mixtures were diluted 12-fold before addition to Vero E6 cell monolayer in 96-well-plate. For each drug concentration, virus-drug mixtures were added to 10 replicate wells at 100 µl per well. The final titer of virus added to cells was 1 x 10^3 $TCID_{50}$/ml (100 $TCID_{50}$ per 100 ul per well in 96-well-plate). After two hours of infection, virus-drug inoculum was replaced with fresh DMEM medium containing 1% FBS. Clear CPE developed after two days of incubation at 37˚C with 5% CO_2. The experiment was repeated thrice. Wells with clear CPE were counted positive and percentage of positive wells for each concentration of tested drugs were plotted. The effect of thiol-based drugs on Vero E6 cells during the two hours of SARS-CoV-2 infection was evaluated by addition of 8.33 mM or 0.52 mM of each drug and 100 $TCID_{50}$ SARS-CoV-2 simultaneously to Vero E6 cell monolayer in 96-well-plate. After two hours of infection, cells were washed and then cultured with fresh DMEM medium containing 1% FBS at 37˚C with 5% CO_2. Clear CPE developed two days post infection.

Quantification of cell viability

The cell viability was quantified using CellTiter-Glo2.0 assay (Promega) which measures cellular ATP content, indicating the metabolically active cells. For all cell viability experiments, the experimental protocol was the same as the main experiment except for the step of pseudovirus/live virus infection. For cell viability measurement corresponding to pseudovirus experiment, 293T-ACE-TMPRSS2 cells were seeded in 96 well black plates 18 hours prior to the experiment. The cells were then incubated with different concentrations (0.02 -1.5mM) of the thiol-based drugs for 2 hours at 37°C, followed by removal of the drugs and incubation of cells with standard culture medium for 18 hours. The experiment was carried out thrice with 5-6 replicates for each drug. These concentrations reflect the 66-fold dilution of drugs when pseudovirus/drug mix was incubated with the cells in the pseudovirus pretreatment setting. For the cell viability measurement corresponding to the live virus experiment, Vero E6 cells were incubated with different concentrations of the drugs (0.03 - 8.33mM) in 1% FBS for 2 days. These concentrations reflect the 12-fold dilution of drugs when virus/drug mix was incubated with the cells in the live virus infection setting. The cell viability experiment on Vero E6 cells was carried out once with 10 replicates for each drug. For both cell viability experiments, post the respective incubations, the plates and their contents were equilibrated at room temperature for 30 minutes before addition of equal volumes of CellTiter Glo2.0 reagent. Afterwards, the contents were mixed on a plate shaker to induce cell lysis. The plates were then incubated at room temperature for 10 minutes followed by measurement of luminescence using Biotek plate reader. Luciferase reads of control-treated cells was set as 100% and the relative viability of cells incubated in the presence of thiol-based drugs was calculated.

Statistical analysis

Statistical significance of difference in loss of binding for each drug was calculated using an ordinary one-way ANOVA, followed by Dunnett's post hoc analysis. For analysis of the effects of the different thiol-based drugs, area under the curve (AUC) was plotted [27] using Graphpad Prism, and ordinary one -way ANOVA followed by Dunnett's posttest was performed. Data are presented as mean ± SEM [* $p \leq 0.05$, ** $p \leq 0.01$, *** $p \leq 0.0001$]. IC_{50} of the drugs in pseudovirus transduction and live virus experiments was determined using the non-linear regression fitting with a variable slope. All statistical analyses were performed using GraphPad Prism software (version 8.4.2).

List of Supplementary Materials

The supplementary file contains two figures (Figures S1 – S4) and a table (Table S1).

References

1. Wiersinga, W. J., Rhodes, A., Cheng, A. C., Peacock, S. J. & Prescott, H. C. Pathophysiology, Transmission, Diagnosis, and Treatment of Coronavirus Disease 2019 (COVID-19): A Review. *JAMA - Journal of the American Medical Association* (2020). doi:10.1001/jama.2020.12839
2. Zhu, N. *et al.* A novel coronavirus from patients with pneumonia in China, 2019. *N. Engl. J. Med.* **382**, 727–733 (2020).
3. Hoffmann, M. *et al.* SARS-CoV-2 Cell Entry Depends on ACE2 and TMPRSS2 and Is

Blocked by a Clinically Proven Protease Inhibitor. *Cell* **181**, 271-280.e8 (2020).

4. Weissenhorn, W. *et al.* Structural basis for membrane fusion by enveloped viruses. *Mol. Membr. Biol.* **16**, 3–9 (1999).

5. Gallagher, T. M. Murine coronavirus membrane fusion is blocked by modification of thiols buried within the spike protein. *J. Virol.* **70**, 4683–4690 (1996).

6. Wong, S. K., Li, W., Moore, M. J., Choe, H. & Farzan, M. A 193-Amino Acid Fragment of the SARS Coronavirus S Protein Efficiently Binds Angiotensin-converting Enzyme 2. *J. Biol. Chem.* **279**, 3197–3201 (2004).

7. Lavillette, D. *et al.* Significant redox insensitivity of the functions of the SARS-CoV spike glycoprotein: Comparison with HIV envelope. *J. Biol. Chem.* **281**, 9200–9204 (2006).

8. Ryser, H. J. P., Levy, E. M., Mandel, R. & DiSciullo, G. J. Inhibition of human immunodeficiency virus infection by agents that interfere with thiol-disulfide interchange upon virus-receptor interaction. *Proc. Natl. Acad. Sci. U. S. A.* **91**, 4559–4563 (1994).

9. Wallin, M., Ekström, M. & Garoff, H. Isomerization of the intersubunit disulphide-bond in Env controls retrovirus fusion. *EMBO J.* **23**, 54–65 (2004).

10. Abell, B. A. & Brown, D. T. Sindbis virus membrane fusion is mediated by reduction of glycoprotein disulfide bridges at the cell surface. *J. Virol.* **67**, (1993).

11. Gallina, A. *et al.* Inhibitors of protein-disulfide isomerase prevent cleavage of disulfide bonds in receptor-bound glycoprotein 120 and prevent HIV-1 entry. *J. Biol. Chem.* **277**, 50579–50588 (2002).

12. Hati, S. & Bhattacharyya, S. Impact of Thiol-Disulfide Balance on the Binding of Covid-19 Spike Protein with Angiotensin-Converting Enzyme 2 Receptor. *ACS Omega* **5**, 16292–16298 (2020).

13. Horowitz, R. I., Freeman, P. R. & Bruzzese, J. Efficacy of glutathione therapy in relieving dyspnea associated with COVID-19 pneumonia: A report of 2 cases. *Respir. Med. Case Reports* **30**, (2020).

14. Akerlund, B. *et al.* Effect of N-acetylcysteine(NAC) treatment on HIV-1 infection: a double-blind placebo-controlled trial. *Eur. J. Clin. Pharmacol.* **50**, 457–61 (1996).

15. Lobo-Galo, N., Terrazas-López, M., Martínez-Martínez, A. & Díaz-Sánchez, Á. G. FDA-approved thiol-reacting drugs that potentially bind into the SARS-CoV-2 main protease, essential for viral replication. *J. Biomol. Struct. Dyn.* (2020). doi:10.1080/07391102.2020.1764393

16. Lan, J. *et al.* Structure of the SARS-CoV-2 spike receptor-binding domain bound to the ACE2 receptor. *Nature* **581**, 215–220 (2020).

17. Wang, Q. *et al.* Structural and Functional Basis of SARS-CoV-2 Entry by Using Human ACE2. *Cell* **181**, 894-904.e9 (2020).

18. Madu, I. G., Belouzard, S. & Whittaker, G. R. SARS-coronavirus spike S2 domain flanked by cysteine residues C822 and C833 is important for activation of membrane fusion. *Virology* **393**, 265–271 (2009).

19. Houk, J., Singh, R. & Whitesides, G. M. Measurement of Thiol-Disulfide Interchange

Reactions and Thiol pKa Values. *Methods Enzymol.* **143**, 129–140 (1987).

20. Nagy, P. Kinetics and mechanisms of thiol-disulfide exchange covering direct substitution and thiol oxidation-mediated pathways. *Antioxidants and Redox Signaling* **18**, 1623–1641 (2013).

21. Atallah, C., Charcosset, C. & Greige-Gerges, H. Challenges for cysteamine stabilization, quantification, and biological effects improvement. *J. Pharm. Anal.* (2020). doi:10.1016/j.jpha.2020.03.007

22. Ariceta, G., Giordano, V. & Santos, F. Effects of long-term cysteamine treatment in patients with cystinosis. *Pediatric Nephrology* **34**, 571–578 (2019).

23. Andreassen, C. N., Grau, C. & Lindegaard, J. C. Chemical radioprotection: A critical review of amifostine as a cytoprotector in radiotherapy. *Semin. Radiat. Oncol.* **13**, 62–72 (2003).

24. Riddles, P. W., Blakeley, R. L. & Zerner, B. Ellman's reagent: 5,5′-dithiobis(2-nitrobenzoic acid)-a reexamination. *Anal. Biochem.* **94**, 75–81 (1979).

25. Pettersen, E. F. *et al.* UCSF Chimera - A visualization system for exploratory research and analysis. *J. Comput. Chem.* **25**, 1605–1612 (2004).

26. Reed, L. J. & Muench, H. A simple method of estimating fifty percent endpoints. *Am. J. Epidemiol.* **27**, 493–497 (1938).

27. Huang, S. & Pang, L. Comparing Statistical Methods for Quantifying Drug Sensitivity Based on *In Vitro* Dose–Response Assays. *Assay Drug Dev. Technol.* **10**, 88–96 (2012).

Acknowledgments: The authors thank Chris Gralapp for drawing Figure 2a and Stefan Oscarson (University College Dublin, Ireland) and Thomas Duff (University College Dublin, Ireland) for helpful discussions about the chemistry of thiol-based drugs.

The following reagent was deposited by the Centers for Disease Control and Prevention and obtained through BEI Resources, NIAID, NIH: SARS-Related Coronavirus 2, Isolate USA-WA1/2020,NR-52281.

Funding: This work was funded by an intramural grant from UCSF (The COVID-19 Rapid Response Pilot Grant Initiative Funding Collaborative) and the US National Institutes of Health (P01 HL128191).

Author contributions:

Kritika Khanna: Conceptualization; methodology; visualization; writing - original draft; writing - reviewing and editing.

Wilfred Raymond: Conceptualization; methodology; visualization; writing - reviewing and editing.

Annabelle R. Charbit: methodology; visualization; writing - reviewing and editing.

Jing Jin: methodology; writing - reviewing and editing.

Irina Gitlin: Conceptualization; writing - reviewing and editing.

Monica Tang: Methodology.

Hannah S. Sperber: Methodology.

Sergej Franz: Methodology.

Satish Pillai: Writing - reviewing and editing.

Graham Simmons: Supervision; methodology; writing - reviewing and editing.

John V. Fahy: Conceptualization; supervision; methodology; visualization; writing - original draft; writing - reviewing and editing.

Competing interests: John Fahy, Irina Gitlin and Wilfred Raymond are inventors on patent applications related to use of thiol-based drugs as treatments for mucus pathology and COVID19. The other authors have no competing interests.

Data and materials availability: All data is available in the main text or the supplementary materials.

Table 1: Comprehensive list of thiol-based drugs or drugs that generate a thiol-containing metabolite*

	Compound	Structure	pKa** (thiol group)
Monothiol drugs			
1	N-acetylcysteine	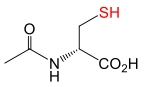	9.5
2	2-mercaptoethane sulfonate, sodium salt (MESNA)	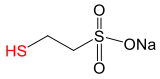	9.2
3	Tiopronin	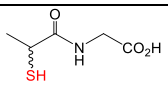	8.7
4	Cysteamine	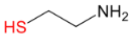	8.2
5	Amifostine (parent drug) WR-1065 (active metabolite)	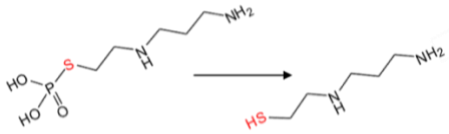	7.7 (WR-1065)
6	Erdosteine (parent drug) Met I (active metabolite)	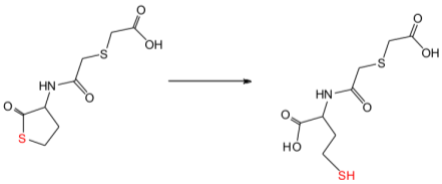	Not available¥
7	Penicillamine	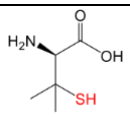	10.5
8	Glutathione	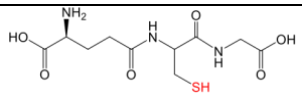	9.2
Dithiol drugs			
9	Bucillamine	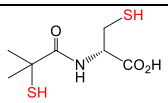	8.4, 10.2
10	Dimercaptosuccinic acid (DMSA) (Succimer)	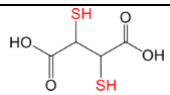	8.9, 10.8
11	2,3-Dimercaprol	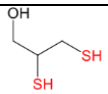	8.6, 10.6
Sulfide drug (Negative Control)			
12	Carbocysteine	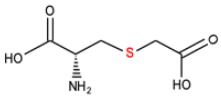	

* Not shown are three thiol containing drugs (Captopril, Zofenopril and Racecadotril) in which primary mechanisms of action is not through reactions or interactions of the thiol group

**pKa values from published literature and PubChem
¥ Literature value not found; pKa ~9-10 is anticipated based on structure

Figure 1

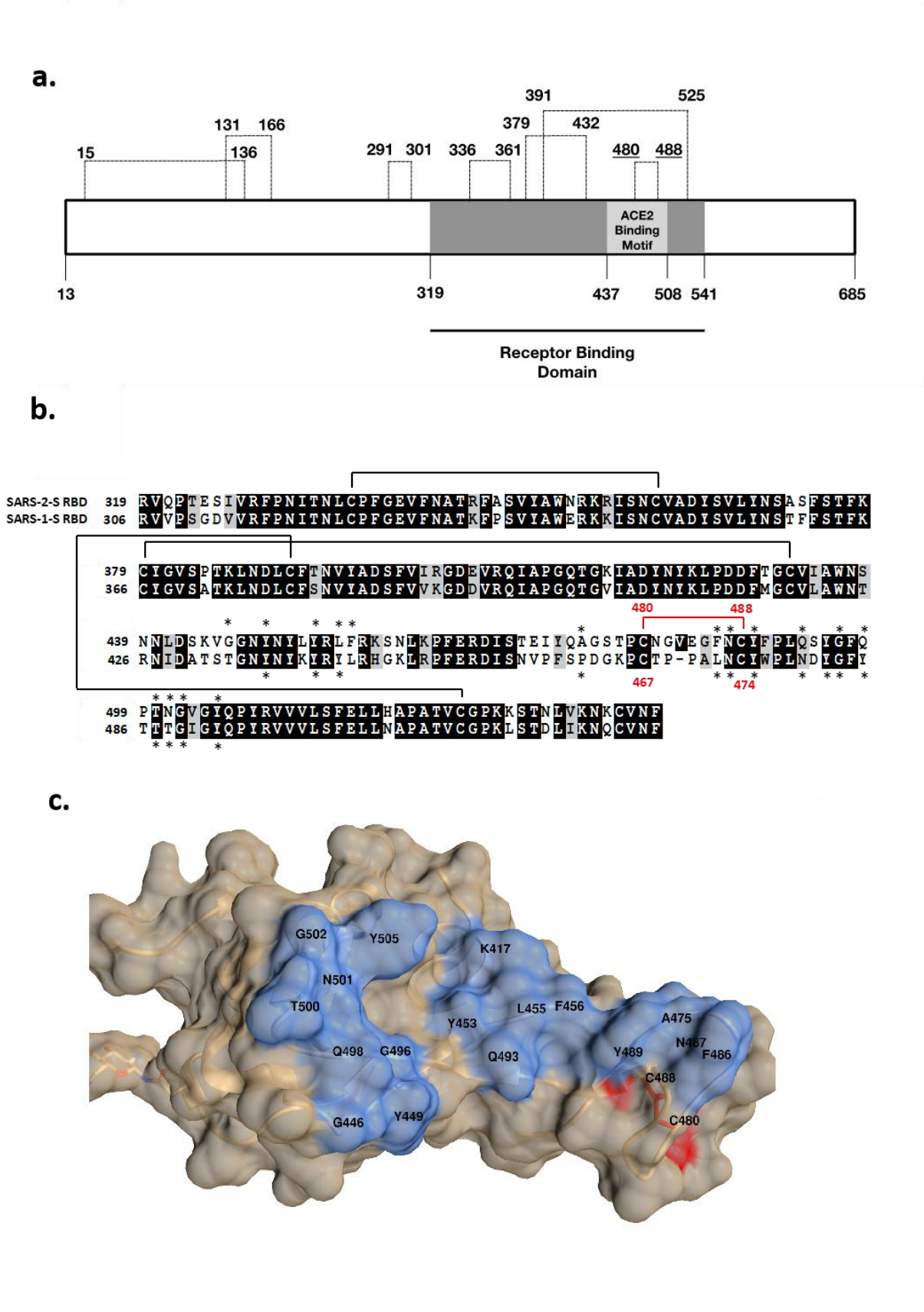
a.
391
525
131
166
379
432
15
136
291
301
336
361
480
488
ACE2
Binding
Motif
13
319
437
508
541
685
Receptor Binding
Domain
b.
SARS-2-S RBD 319 RVQPTESIVRFPNITNLCPFGEVFNATRFASVYAWNRKRISNCVADYSVLYNSASFSTFK
SARS-1-S RBD 306 RVVPSGDVVRFPNITNLCPFGEVFNATKFPSVYAWERKKISNCVADYSVLYNSTFFSTFK
379 CYGVSPTKLNDLCFTNVYADSFVIRGDEVRQIAPGQTGKIADYNYKLPDDFTGCVIAWNS
366 CYGVSATKLNDLCFSNVYADSFVVKGDDVRQIAPGQTGVIADYNYKLPDDFMGCVLAWNT
480
488
439 NNLDSKVGGNYNYLYRLFRKSNLKPFERDISTEIYQAGSTPCNGVEGFNCYFPLQSYGFQ
426 RNIDATSTGNYNYKYRYLRHGKLRPFERDISNVPFSPDGKPCTP-PALNCYWPLNDYGFY
467
474
499 PTNGVGYQPYRVVVLSFELLHAPATVCGPKKSTNLVKNKCVNF
486 TTTGIGYQPYRVVVLSFELLNAPATVCGPKLSTDLIKNQCVNF
c.
G502
Y505
K417
N501
T500
L455
F456
Y453
A475
N487
Q498
G496
Q493
Y489
F486
C488
G446
Y449
C480

Figure 1. Cystine mapping and conservation of cystines in beta coronavirus RBD. Panel (a): Cystine map for SARS-2-S domain S1, amino acids 15 – 685, comprising the sequence from the mature N-terminus to the first TMPRSS2 proteolytic site R685 (UniProt Entry: P0DTC2). Seven cystine linkages are denoted by dashed lines with amino acid residue number above. The dark gray region is the receptor binding domain (RBD), and the lighter gray box highlights the ACE2 binding motif, a cluster of amino acids that make contact with ACE2. Panel (b): Amino acid alignment of SARS-2-S RBD domain (aa 319-541, PDB Entry 6M0J) and SARS-1-S RBD domain (aa 306-517, PDB Entry 3SCI). Residues that are shared are highlighted by black boxes and residues that represent a similar amino acid class replacement are bound by gray boxes. The solid lines link cystine-forming cysteines. The solid red line and red numbers highlight the conserved cystine bridge in the RBDs for both viruses. Asterisks denote amino acids that are within 4 angstroms of ACE2 in their respective solved structures. Panel (c): A surface rendering of SARS-2-RBD (PDB Entry 6M0J) generated with UCSF Chimera software oriented with the ACE2 binding region (blue) facing forward. Amino acids are noted with single letter code and sequence number. The conserved RBD cystine formed by C480 and C488 is highlighted in red.

Figure 2

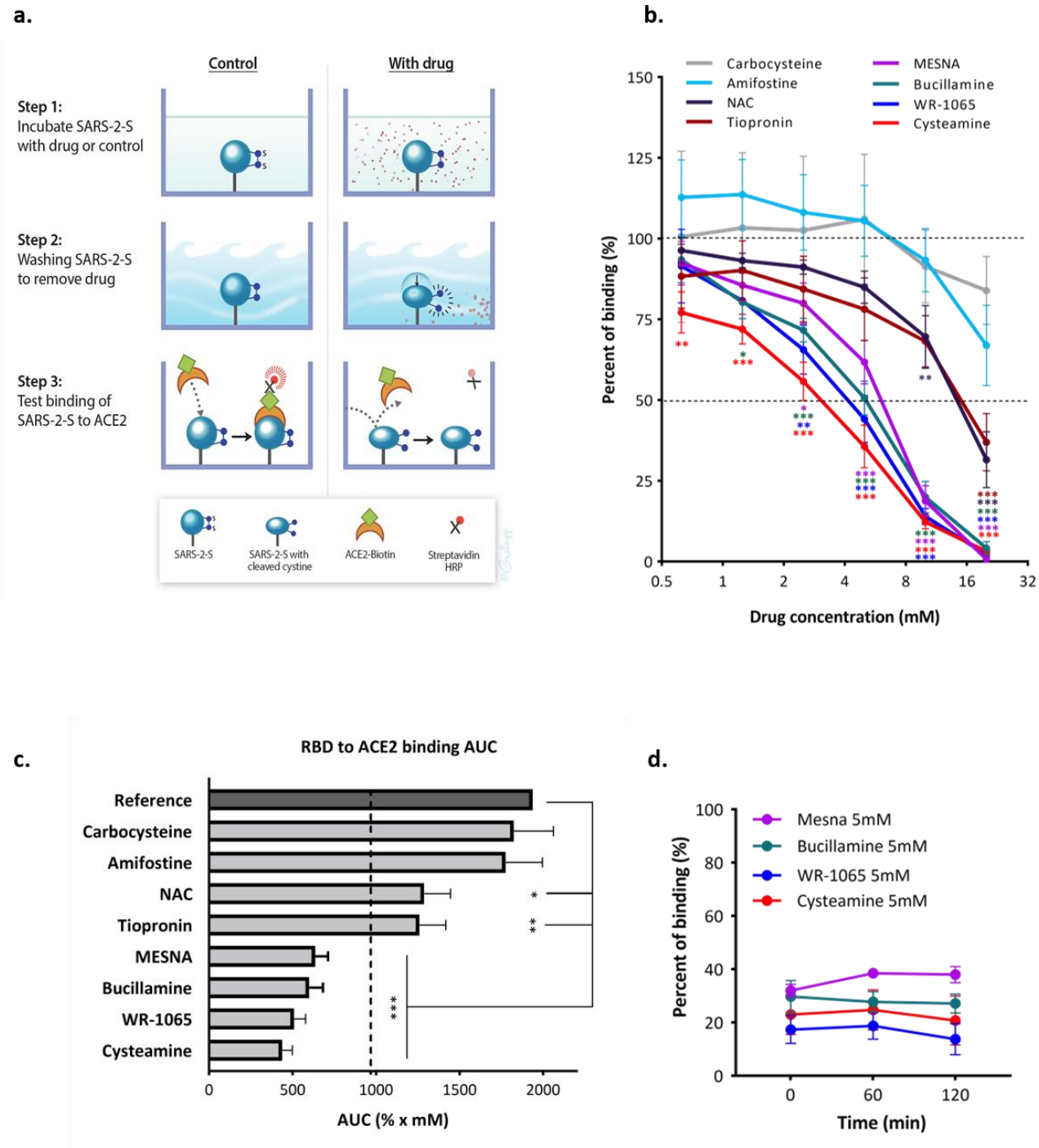
a.
Control
With drug
Step 1:
Incubate SARS-2-S with drug or control
Step 2:
Washing SARS-2-S to remove drug
Step 3:
Test binding of SARS-2-S to ACE2
SARS-2-S
SARS-2-S with cleaved cystine
ACE2-Biotin
Streptavidin HRP
b.
Carbocysteine
Amifostine
NAC
Tiopronin
MESNA
Bucillamine
WR-1065
Cysteamine
Percent of binding (%)
Drug concentration (mM)
c.
RBD to ACE2 binding AUC
Reference
Carbocysteine
Amifostine
NAC
Tiopronin
MESNA
Bucillamine
WR-1065
Cysteamine
AUC (% x mM)
d.
Mesna 5mM
Bucillamine 5mM
WR-1065 5mM
Cysteamine 5mM
Percent of binding (%)
Time (min)

Figure 2. Binding of SARS-CoV-2 RBD to ACE2 is inhibited by thiol-based drugs. Panel (a): Schematic representation of the SARS CoV-2 RBD to ACE2 binding assay. RBD was covalently coupled to plates functionalized with primary amine-reactive maleic anhydride. ACE2 binding was then evaluated after RBD exposure to thiol-based drugs for 60 minutes. Panel (b) shows percent of binding in the presence of the drugs (n = 4 - 6). Without drug treatment, the binding was 100%, whereas treatment with the thiol-based drugs showed a decrease in the binding % relative to no drug control. The X axis is scaled to log2. Panel (c) shows area under the curve (AUC) analysis for effects of the thiol-based drugs on RBD to ACE2 binding. Reference AUC was calculated from RBD to ACE2 binding with no drug control; dashed line represents 50% of reference AUC. Panel (d) shows binding of RBD to ACE2 at one and two hours post WR-1065, cysteamine, Mesna or bucillamine exposure and washout (n = 4 - 5). Data are mean ± SEM. Statistical significance was analyzed by one-way ANOVA followed by Dunnett's post-hoc analysis. Significance indicates differences from no drug control (c) or reference AUC (d). *$p \leq 0.05$, **$p \leq 0.01$, ***, $p \leq 0.0001$.

Figure 3

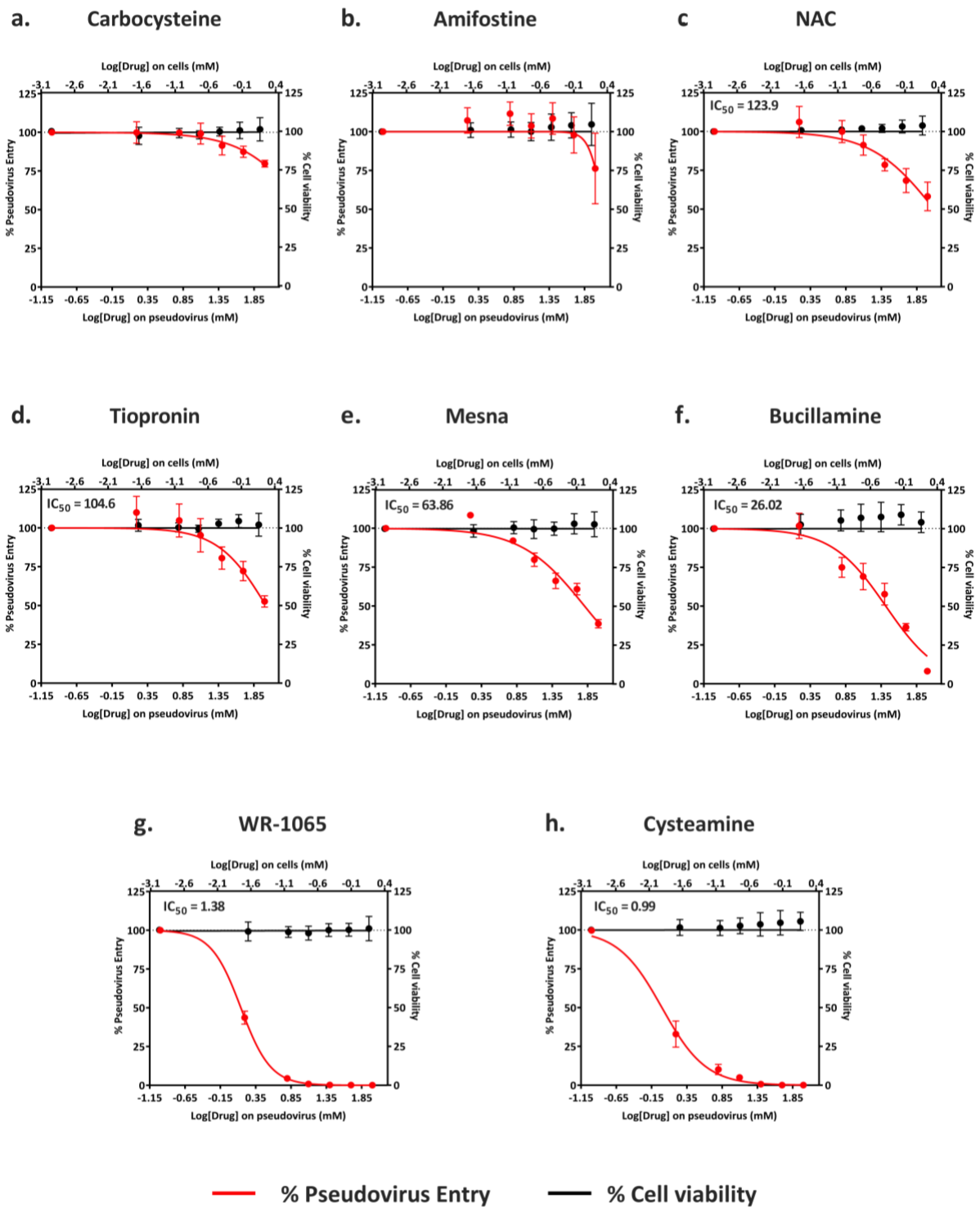
a. Carbocysteine
b. Amifostine
c NAC
IC50 = 123.9
d. Tiopronin
IC50 = 104.6
e. Mesna
IC50 = 63.86
f. Bucillamine
IC50 = 26.02
g. WR-1065
IC50 = 1.38
h. Cysteamine
IC50 = 0.99
Log[Drug] on cells (mM)
Log[Drug] on pseudovirus (mM)
% Pseudovirus Entry
% Cell viability
% Pseudovirus Entry
% Cell viability

Figure 3. **Entry of SARS-CoV-2 pseudoviruses into 293T-ACE2-TMPRSS2 cells is inhibited by thiol-based drugs.** Pseudovirus (PV) entry efficiency, quantified by luciferase activity, when the pseudoviruses were exposed to thiol-based drugs prior to cell transduction (as illustrated in Figure S1) (n = 3-4). The effects of drugs on 293T-ACE2-TMPRSS2 cell viability was quantified using Cell Titer Glo 2.0 with lower drug dose exposures, reflecting 66-fold dilution of drugs when pseudovirus/drug mixture was incubated with cells. X-axes are scaled to log10 - the lower X-axis refers to concentration of drugs on the pseudovirus and the upper X-axis refers to equivalent concentration of drugs on the cells. The left Y-axis refers to PV entry efficiency and the right Y-axis refers to cell viability. Percentage changes are with respect to no drug control which is set as 100%. The Data are mean ± SD.

Figure 4

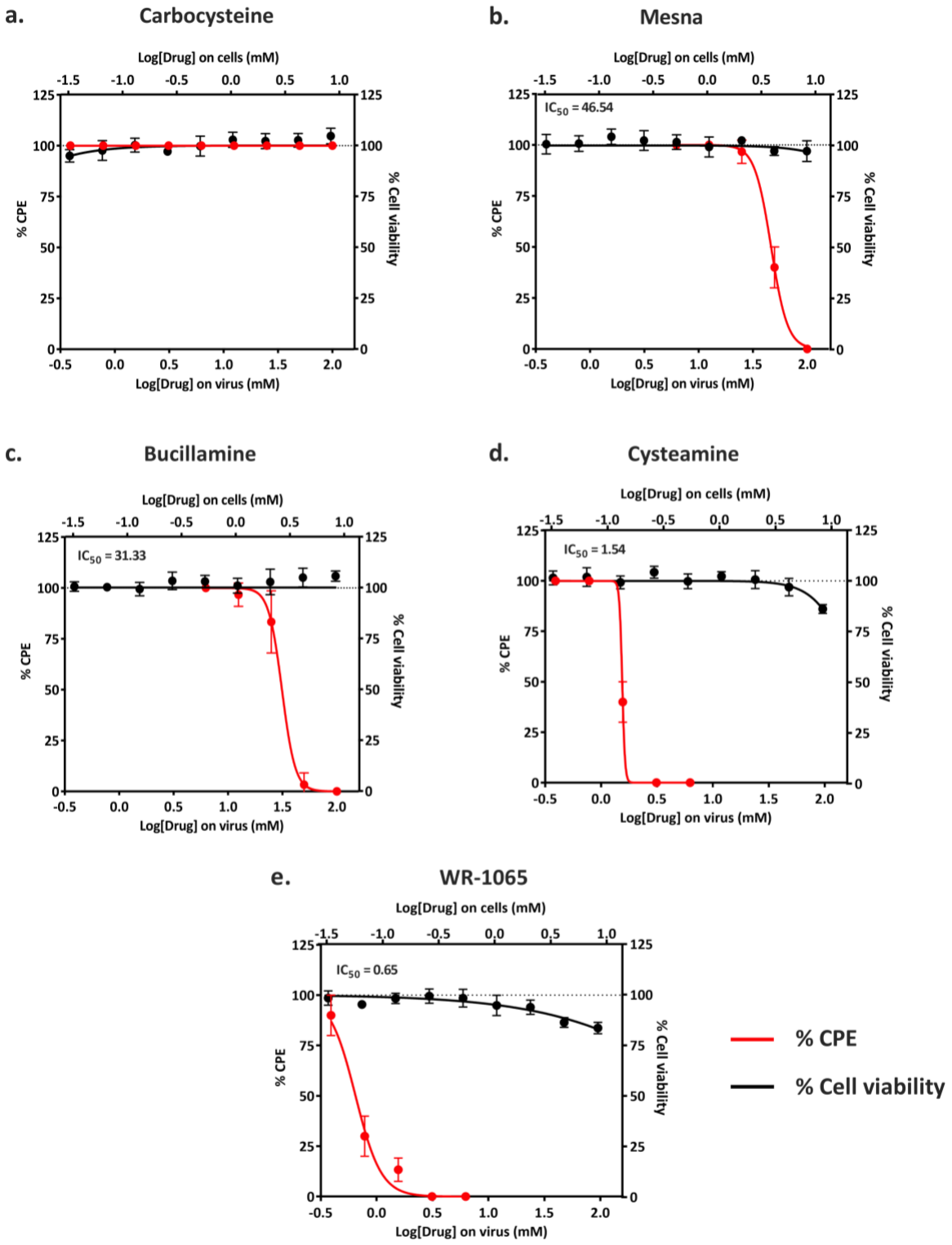
a.
Carbocysteine
b.
Mesna
IC50 = 46.54
c.
Bucillamine
IC50 = 31.33
d.
Cysteamine
IC50 = 1.54
e.
WR-1065
IC50 = 0.65
Log[Drug] on cells (mM)
Log[Drug] on virus (mM)
% CPE
% Cell viability
% CPE
% Cell viability

Figure 4: Thiol-based drugs inhibit SARS-CoV-2 virus infectivity in VeroE6 cells. Cytopathic effects (CPE) quantified by visual inspection when virus is exposed to drugs prior to cell infection (n = 3). The effects of drugs on Vero E6 cell viability was quantified using Cell Titer Glo 2.0 with exposure of cell to lower drug doses, reflecting the 12-fold dilution of drugs when virus/drug mixture was incubated with cells. The X-axes are scaled to log10 - the lower X-axis refers to the concentration of drugs on the virus and the upper X-axis refers to equivalent concentration of drugs on the cells. The left Y-axis refers to cytopathic effects and the right Y-axis refers to cell viability. Percentage changes are with respect to no drug control which is set as 100%. Data are mean ± SD.